Controlling the growth and shape of chiral supramolecular polymers in water

Pol Besenius[a], Giuseppe Portale[b], Paul H. H. Bomans[c], Henk M. Janssen[d], Anja R. A. Palmans[a], and E. W. Meijer[a,1]

[a]Institute of Complex Molecular Systems and Laboratory of Macromolecular and Organic Chemistry, Eindhoven University of Technology, P.O. Box 513, 5600 MB Eindhoven, The Netherlands; [b]Dutch-Belgian Beamline 26 (DUBBLE BM26), European Synchrotron Radiation Facility (ESRF), 6, Rue Jules Horowitz, BP220, 38043 Grenoble, France; [c]Laboratory of Materials and Interface Chemistry and Soft Matter CryoTEM Research Unit, Department of Chemical Engineering and Chemistry, Eindhoven University of Technology, P.O. Box 513, 5600 MB Eindhoven, The Netherlands; and [d]SyMO-Chem, P.O. Box 513, 5600 MB Eindhoven, The Netherlands

A challenging target in the noncovalent synthesis of nanostructured functional materials is the formation of uniform features that exhibit well-defined properties, e.g., precise control over the aggregate shape, size, and stability. In particular, for aqueous-based one-dimensional supramolecular polymers, this is a daunting task. Here we disclose a strategy based on self-assembling discotic amphiphiles that leads to the control over stack length and shape of ordered, chiral columnar aggregates. By balancing out attractive noncovalent forces within the hydrophobic core of the polymerizing building blocks with electrostatic repulsive interactions on the hydrophilic rim we managed to switch from elongated, rod-like assemblies to small and discrete objects. Intriguingly this rod-to-sphere transition is expressed in a loss of cooperativity in the temperature-dependent self-assembly mechanism. The aggregates were characterized using circular dichroism, UV and 1H-NMR spectroscopy, small angle X-ray scattering, and cryotransmission electron microscopy. In analogy to many systems found in biology, mechanistic details of the self-assembly pathways emphasize the importance of cooperativity as a key feature that dictates the physical properties of the produced supramolecular polymers.

aqueous self-assembly | controlled architecture | supramolecular polymerization | dynamic materials

Molecular self-assembly has emerged as a fascinating area in its own right (1, 2). A toolbox initially developed by supramolecular chemists quickly expanded into an interdisciplinary field aiming at the manipulation of matter at the molecular scale (3, 4). Up until recently self-assembly in dilute aqueous environments has predominantly dealt with linear amphiphiles that form closed structures (5–9), such as spherical micelles, cylindrical or rod-like micelles, and vesicles using, for example, phospholipids (10, 11), synthetic block copolymers (12, 13), or dendrimers (14). Morphological control in objects of defined size or shape, and transitions between different morphologies are increasingly well understood (15–18). Surprisingly, however, the generality of these concepts has not been translocated into another area of increasing interest, namely, the self-assembly of one-dimensional arrays. In that context the development of discotic monomers has proven to be a valuable route to allow for the synthesis of rod-like supramolecular polymers (19), whose potential applications in functional soft matter include electronics, biomedical engineering, and sensors (20–26). Considering the enormous interest in such systems, it is surprising that efforts to control the size and shape of nano- and micrometer size one-dimensional objects are rare (27–29); successful strategies rely on the use of templates (30, 31), end cappers (32), or selective solvent techniques (33).

In order to control the growth of aqueous one-dimensional supramolecular polymers, we propose to utilize electrostatic repulsive contributions in analogy to surfactant type self-assembly. However, rather than simply relying on solvophobic effects based on the lipophilic segments of the amphiphile, we use noncovalent polymerizable moieties to craft building blocks that are designed to code for "infinitely" long, chiral supramolecular architectures. Along with others (22, 28, 29, 34, 35), we are convinced that exploring the balance between attractive forces (dipole interactions, π-π stacking, and solvophobic effects) and repulsive interactions allows us to produce supramolecular materials with well-defined architectures and order parameters over several length scales. On the basis of that hypothesis, we hereby report a strategy to rationally control the shape, size, and stability of columnar assemblies in aqueous environments using subtle differences in the ionic character of C_3-symmetrical discotic amphiphiles. This is a unique example for directional self-assembly in water whereby the supramolecular polymer shape and size can be dictated by Coulombic interactions. In line with our continuous efforts in elucidating the mechanisms of supramolecular polymerizations (36, 37), we have focused on correlating the morphological properties of the produced materials with the appropriate mechanistic details of the self-assembly pathways.

Results and Discussion

Design Concept and Synthesis. The hydrophobic effect between insoluble apolar moieties and the steric and/or electrostatic repulsion in the polar head group are generally the major governing forces in the aqueous self-assembly of linear amphiphiles. The competition between those opposing forces, which itself is depending on the relative geometry of both moieties—the surfactant packing parameter—dictates the resultant morphology of the structures (10, 11). Mukerjee et al. (38) and Tanford (39) pioneered the idea of repulsive interactions between polar surfactant head groups being the dominant forces that constrain micelles to finite sizes. In analogy we propose the use of repulsive Coulombic forces in order to control the aqueous supramolecular polymerization of discotic amphiphiles into columnar assemblies of defined length.

The molecular design of our self-assembling unit is based on the well-studied C_3-symmetrical benzene-1,3,5-tricarboxamide (BTA) core that directs the self-assembly into triple hydrogen-bonded helices (40–42). This moiety was extended with a fluorinated L phenylalanine and an aminobenzoate spacer, thereby significantly increasing the stability of the assemblies via additional hydrogen bonding, π-π interactions, and solvophobic effects (Fig. 1), while at the same time creating a hydrophobic pocket in the core of the discotic to shield the triple hydrogen-bonding motif. Our reason for introducing peripheral hydrophilic metal chelates complexes was twofold: A divergent synthetic approach
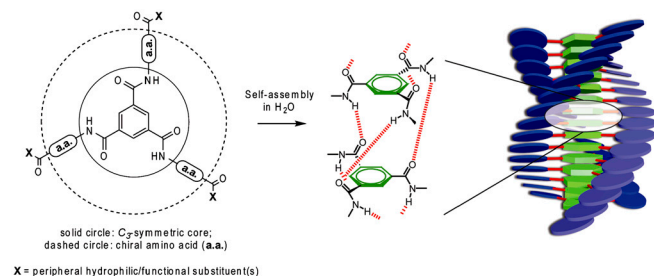
Fig. 1. Schematic representation of the self-assembly of discotic amphiphiles: The hydrophobic BTA core (solid circle) directs the self-assembly into a helical architecture; the hydrophobic, chiral amino acid substituents (dashed line) in the second layer determine the handedness and stability of the helix; the peripheral hydrophilic groups introduce an amphiphilic character to the design.

for the C_3-symmetrical discotics allowed the synthesis of three amphiphiles with increasing ionic character from a common intermediate (*SI Appendix*). At the same time complexation of a paramagnetic lanthanide, e.g. Gd(III), would open the route for the preparation of a unique class of supramolecular contrast agents for magnetic resonance imaging (Fig. 2).

A common synthetic intermediate for all three discotic amphiphiles **1–3** was synthesized in four high yielding steps via standard amide coupling reactions using orthogonal protecting groups (*SI Appendix*). Thereafter two to three synthetic steps were necessary to couple the appropriate ligands onto the common intermediate, followed by complexation with the trivalent metal to yield the final discotic amphiphiles (*SI Appendix*). Compound **1** (Fig. 2) is based on the M(III)-DOTA (1,4,7,10-tetraazacyclodo-decane-N,N′,N″,N‴-tetraacetic acid) monoamide chelate, an overall charge-neutral complex. By switching to a DTPA (diethy-lenetriaminepentaacetic acid) derivative linked via one of the car-boxylic acids, we introduce one remaining negative charge per chelated metal or three per discotic (**2**, Fig. 2). If the linker is attached to the ethylene bridge of the DTPA chelater, the com-plexation of a trivalent metal at close to neutral pH leads to two overall remaining charges per complex and the necessity for two counter cations (**3**, Fig. 2).

By increasing the ionic character of the peripheral M(III) com-plexes, we are aiming to introduce frustration in the one-dimen-sional growth of the stacks, an intriguing concept for discotic monomers whose core is designed to code for elongated rod-like aggregates. The motivation of the present work is to control the length and aspect ratio of the helical columnar self-assemblies, and we therefore focus the first part of our investigations on mor-phological characterization of the one-dimensional supramolecu-lar polymers in aqueous solution.

Shape and Size of the Supramolecular Aggregates. A powerful tech-nique to determine the shape and size of colloidal dilute particu-late systems is small angle scattering (43–47). The presence of peripheral metal complexes strongly increased the scattering power of the aggregates and enabled the investigation of dilute solutions by means of synchrotron small angle X-Ray scatter-ing (SAXS).

Fig. 3 reports the SAXS profiles for the discotic amphiphiles **1a** and **3a** in citrate buffer solutions at different concentrations.* The shape of the aggregates can be directly derived from the slope of the SAXS profiles in the region $0.01 < q < 0.06$ Å^{-1}. Discotic **1a**-based aggregates clearly show a q^{-1} slope (Fig. 3*A*), characteristic of rod-like objects. The aggregates can be described as noninter-acting cylinders, and the profiles were fitted assuming a homoge-

nous monodisperse cylindrical form factor (*SI Appendix*). The calculated rod radii of 3.1 nm are independent of the concentra-tion and in agreement with extended chain structures of the flattened monomeric building blocks ($R \sim 2.9$ nm). The lengths or the rods are 25 nm at lower concentrations and larger than 75 nm at 1 mM.

In contrast, any characteristic slope indicating aggregate shape anisotropy is absent in the SAXS profiles from solutions of dis-cotic **3a** (Fig. 3*B*). The data measured at different concentrations could be fitted using a homogenous monodisperse spherical form factor (see *SI Appendix*), leading to calculated radii of 3.2 nm. Comparison with chain extended structures and a corresponding geometric radius of around 3.0 nm strongly suggests the presence of aggregates with an aspect ratio of close to 1.

By determining diffusion coefficients of the aggregated diamag-netic discotic amphiphile **3b** in a deuterated succinate buffer (50 mM, "pH 6"), the Stoke–Einstein relation (48) allowed us to calculate hydrodynamic radii of the discrete objects of spherical size (Table 1). Their size is in agreement with values obtained from SAXS data for **3a**. Assuming an interdisc distance of 3.5 Å (42), we were able to estimate the weight averaged degrees of polymeriza-tion (DP_W) leading to molecular weights of about 50 kDa at a monomer concentration of 1 mM. On the other hand in the case of diamagnetic discotic **1b**, very extensive line broadening in the ^{1}H-NMR spectra and a complete loss of signals at room tempera-ture resulted from the large degree of polymerization (>200 according to SAXS) of the self-assembled rod-like aggregates.

Final and definite evidence for successful control over one-dimensional stack length was obtained from cryogenic transmis-sion electron microscopy (cryo-TEM) micrographs. The techni-que preserves the structural morphology of the self-assembled aggregates and avoids drying affects related to conventional TEM sample preparation. Rod-like morphologies are visible for supramolecular polymers based on building block **1a** (Fig. 4). The 5-nm width of the rods are in good agreement with the SAXS data. In contrast, Fig. 5 shows that discotic **3a** did produce the expected spherical objects with dimensions close to 5 nm at a 1-mM building block concentration (Fig. 6), which confirms the results from SAXS and diffusion ordered spectroscopy (DOSY) measurements. According to these findings, we have been able to obtain self-assembled discrete objects that can be considered the supramolecular equivalent of dendritic macromo-lecules (49, 50).

Similarly to the self-assembly of linear amphiphiles we have used Coulombic interactions to introduce repulsive forces and restrict one-dimensional growth of supramolecular polymers. We are, however, not content with only determining the morphol-ogies of the produced materials in solution. In order to fully investigate the governing forces in the aqueous self-assembly of discotic amphiphiles, we used spectroscopic data to elucidate the order in the columnar aggregates and study the mechanism by which the polymers grow via temperature-dependent measure-ments. In a recent review, we have emphasized the importance of differentiating self-assembly mechanisms for supramolecular polymers in analogy to the classification of traditional covalent polymers (36).

Self-Assembly Mechanism. Optical spectroscopy has in the past pro-ven to be a rich experimental source for elucidating the order in and structure of self-assembled systems (20, 41, 51–53). Circular dichroism (CD) spectroscopic data, in particular, show bisignate cotton effects for all three compounds in the same citrate buffer (100 mM, pH 6), which strongly suggest the presence of ordered aggregates (Fig. 7): We can therefore reliably postulate the formation of helical assemblies. Note that in order to make fair comparisons between the different compounds and at the same time relate the results of the optical measurements to the SAXS data, as well as the cryo-TEM micrographs, we used the same

---

*Compound **2** was not soluble enough to enable morphological characterization at high concentrations.
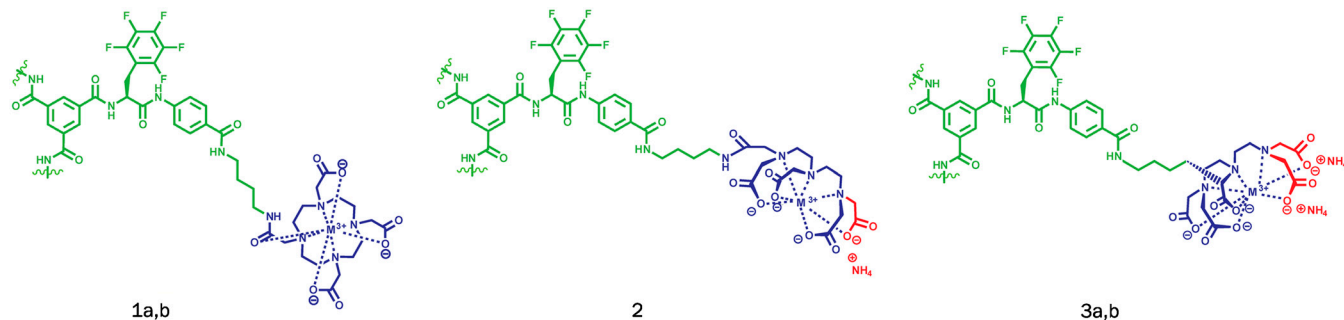
Fig. 2. Schematic representations of the fluorinated discotic amphiphiles: the BTA core, chiral amino acid (*L* pentafluorophenylalanine), and aminobenzoate spacer are schematically depicted in green; the peripheral hydrophilic M(III) complexes (depicted in blue) introduce an increasingly pronounced "ionic character" (depicted in red) to the molecular building blocks: overall neutral M(III)-DOTA **1**, singly charged M(III)-DTPA-*N*-MA **2**, and doubly charged M(III)-DTPA **3** [for paramagnetic discotics **1a**, **2**, and **3a** M(III) = Gd(III); for diamagnetic discotic **1b** and **3b** M(III) = Y(III)].

buffered conditions as described above (100 mM citrate buffer at pH 6).

After heating the buffered solutions to a molecularly dissolved state, we recorded cooling curves and monitored the shape and intensity of the CD and UV/Vis spectra upon polymerization of the supramolecular aggregates (Fig. 7D–F). The extraordinarily high stability of the fluorinated discotic amphiphiles **1a**–**3a** in aqueous buffered environments is indicated by the dilute conditions and very high temperatures required to fully depolymerize the aggregates. The importance of solvophobic effects and hydrophobic shielding become evident when comparing compounds **1a** and **3a** to their nonfluorinated equivalent. Aggregates based on the latter are about an order of magnitude less stable.

Striking is the difference in the cooling curves monitored at λ_{max} of the individual compounds and performed at $1 \ K \cdot min^{-1}$ in order to allow supramolecular polymerization to proceed under thermodynamic control (Fig. 7). The cooling curves for discotics **1a** and **2** are clearly nonsigmoidal, which is indicative for a cooperative temperature dependent self-assembly, that can be described by a nucleation-elongation type mechanism (Fig. 7 *D*

and *E*). Two regimes can be distinguished: a thermodynamically less favored and nonordered nucleation regime at high temperatures, separated from the polymerization or growth regime by T_e, the temperature below which elongation occurs. In strong contrast, compound **3a** led to sigmoidal temperature-dependent profiles with a red-shifting negative CD band upon decreasing the temperature (Fig. 7*F*). There clearly is no positive cooperative mechanism operative, and at least on a macroscopic level—based on temperature-dependent CD profiles—we propose an isodesmic or equal K model to be dominating the self-assembly behavior.

These drastic changes in the supramolecular polymerization mechanisms were confirmed by UV/Vis spectroscopy (*SI Appendix*). The UV bands of the aromatic moieties in the wedge of the discotics shift toward higher wavelengths, a strong indication for the formation of J aggregates or slipped arrangement of the peripheral chromophores. However, the red shifts that were observed upon aggregation are relatively small, and in these cases we prefer to rely on the more sensitive CD cooling curves for fitting procedures.

Various research groups, including ours, have reviewed models that allow the distinction between fundamentally different self-assembly mechanisms (36, 52, 54–56). Based on the van der Schoot model (54), reliable fitting procedures (37) can provide us with the thermodynamic parameters describing the processes involved. For the cooperative self-assembly of compounds **1a** and **2**, above T_e the nucleation regime is characterized by a dimensionless activation constant K_a of 10^{-4} for **1a** and 10^{-3} for **2**. Below T_e the growth regime can be described by the enthalpy change upon elongation (ΔH_e), which is 40 kJ mol^{-1} for both building blocks **1a** and **2**. Another typical characteristic of these enthalpy-driven supramolecular polymerization mechanisms becomes evident when performing concentration-dependent experiments: The T_e values shift to lower temperatures when decreasing the concentration of the monomer (*SI Appendix*).

Assuming an isodesmic mechanism (37, 54) in the self-assembly of compound **3a**, the apparent association constant at 298 K is on the order of $5 \cdot 10^5 \ M^{-1}$ in a concentration regime of 8 μM to 20 μM. Only a slight decrease to $3 \cdot 10^5 \ M^{-1}$ is observed when switching to a 10-mM PBS buffer at pH 7.4 or a 50-mM succinate buffer at pH 6 (*SI Appendix*). The latter became relevant for ^{1}H NMR spectroscopic measurements as its deuterated equivalent is commercially available. Similarly to supramolecular polymers based on **1a** and **2**, melting curves for stacks of **3a** shift to lower temperatures upon dilution (*SI Appendix*).
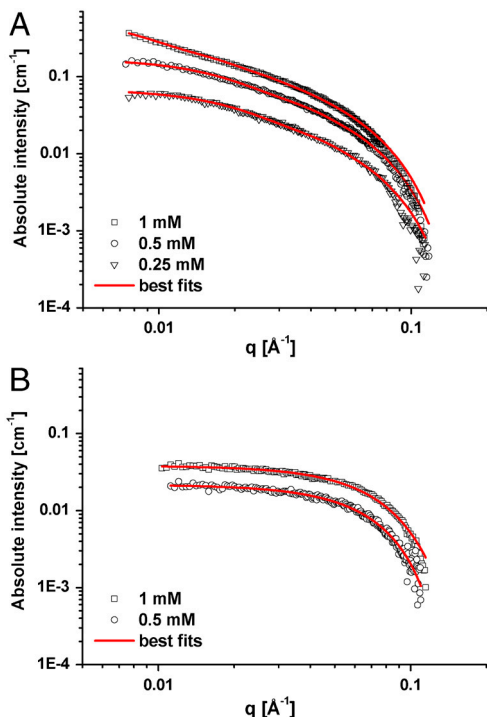

Fig. 3. SAXS profiles for the fluorinated discotics **1a** (*A*) and **3a** (*B*) in citrate buffer (100 mM, pH 6).

Table 1. ^{1}H-DOSY NMR data of stacks based on amphiphile 3b

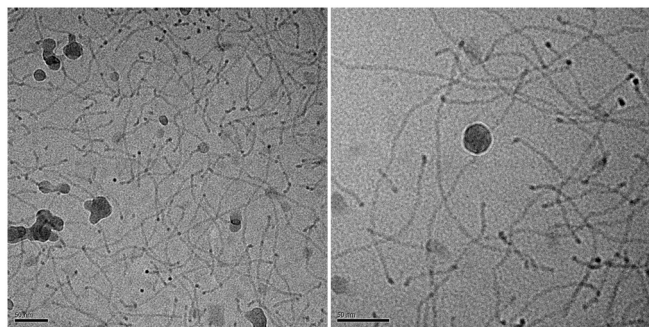| 3b [mM]	D_t (stacks) [10^{-10} m^2 s^{-1}]	R_H (stacks) [10^{-10} m]	DP$_W$
1	0.69	29	17
2	0.38	52	30

Fig. 4. *Cryo*-TEM micrographs for self-assembled discotic amphiphile **1a** (0.66 mM) vitrified at 288 K in citrate buffer (100 mM, pH 6); scale bar represents 50 nm.[†]
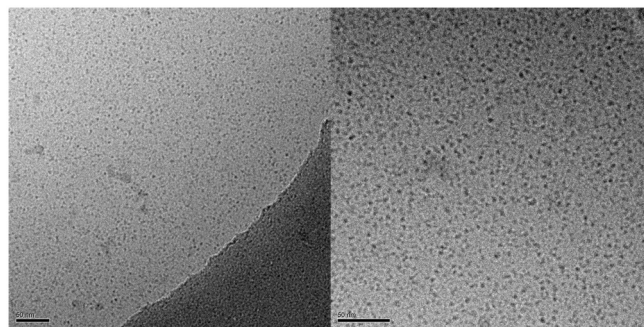

Fig. 5. *Cryo*-TEM micrographs for discotic amphiphile **3a** (1 mM) vitrified at 288 K in citrate buffer (100 mM, pH 6); scale bar represents 50 nm.

Optical measurements strongly suggest that the increased ionic character of discotic amphiphile **3a** compared to compounds **1a** and **2** has led to the intended changes in the self-assembly behavior. Furthermore, we were able to correlate cooperative self-assembly processes to the formation of high molecular weight supramolecular polymers, producing high aspect ratio rod-like aggregates. In contrast, the absence of a cooperative mechanism led to a huge decrease in the degree of polymerization, yielding discrete objects with aspect ratios close to 1. This is in agreement with a theory that predicts a switch to anticooperativity with increased Coulombic repulsive interactions. This anticooperative mechanism is not distinguishable of an isodesmic process. The latter is a step-by-step reversible polycondensation—the equivalent in covalent polymer chemistry—which yields only moderate degrees of polymerization with large polydispersities, unless the binding affinity or conversion is extremely high. Hence, where **1a** and **2** polymerize in a cooperative manner, yielding long elongated rods, the highly charged **3a** polymerizes in an anticooperative manner yielding discrete objects.

This leaves us with finding further evidence for the assumption that solely Coulombic repulsive interactions are responsible for those drastic changes in the observed self-assembly mechanisms.

Frustrated Growth Induced by Coulombic Repulsive Forces. At this stage we should point out that so far we have mainly worked in one specific buffer in order to make meaningful comparisons between various building blocks and characterization techniques. However, if electrostatic repulsive forces of the peripheral charged M(III)-DTPA complexes on discotic **3** are at the origin of the frustrated one-dimensional growth and possibly reduced order within the aggregates, we expected that increasing the ionic strength of the buffered environment, using an inert 1∶1 salt with highly hydrated counterions, should restore cooperative growth. In citrate buffered 0.2 M NaCl, the effect was not yet observed (*SI Appendix*). However, when we increased the salt concentration further to 0.5 M (Fig. 8), the CD spectrum and the shape of the cooling curve (K_a is 10^{-3} and ΔH_e 35 kJ mol^{-1}) were very reminiscent to the corresponding spectral data for the overall charge neutral, cooperatively assembling discotic **1a** (Fig. 7 *A* and *D*). Importantly, the restoration of cooperativity in the self-assembly of charged monomer **3a** was also accompanied by the formation of high aspect ratio rod-like supramolecular polymers, clearly observed in *cryo*-TEM micrographs at high ionic strength (Fig. 9). Electrostatic screening is the most likely explanation for those findings and in line with the disruption of frustrated growth in Hartegrink's multidomain peptide assemblies observed at a salt concentration of 1 M NaCl (28). In the field of linear-charged amphiphiles or ionic surfactant-like self-

assemblies, salt-induced sharp sphere-to-rod micellar transitions were reported already about 20 years ago (57–59). By increasing the ionic strength of the aqueous environment, spherical charged micelles were able to grow into rod- or worm-like micelles at the same surfactant volume fraction. Similarly, polyelectrolytes—covalent macromolecules with charged ionizable groups—can behave like semiflexible polymers with ionic strength-dependent persistence length: Stiff cylinder-like conformations of a polyelectrolyte at low salt concentration can be collapsed into spherical globules or coils via electrostatic screening (60–65). More recently the importance of screening Coulomb interactions has also been reported for the self-assembly of virus capsids (66).

Conclusions

By balancing out attractive forces based on dipole interactions, π-π stacking, solvophobic effects, with electrostatic repulsive interactions, we have managed the self-assembly of discotic amphiphiles into helical, columnar aggregates of controlled length. Whereas the hydrophobic core of the discotic building block determines the high stability of the aggregates, it is the peripheral ionic character of the hydrophilic metal complexes that has a drastic impact on the self-assembly mechanism and the resulting aspect ratio of the nanoscale objects. Subtle changes in the ionic character resulted in the abrupt loss of cooperativity: Coulombic repulsions led to frustrated growth and hence to the formation of objects of discrete size, as opposed to elongated rod-like columnar assemblies. We demonstrated that charge-charge repulsive interactions are the primary forces involved in the case of restricted growth by fully restoring cooperative growth via electrostatic screening.

In summary, the combination of positive molecular interactions on one hand and the use of Coulombic repulsive interactions on the other hand are both an extremely powerful tool in order to gain control over the targeted architectures. This approach paves the way for what we believe to be one of the
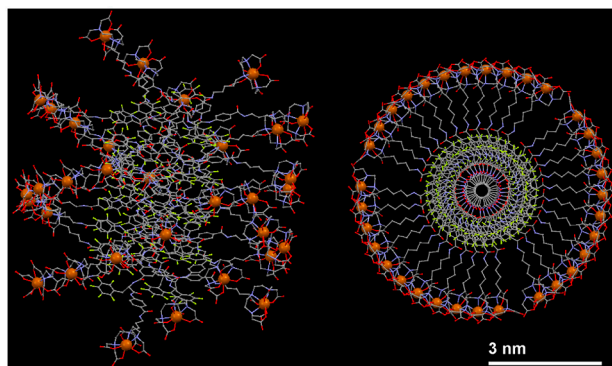

Fig. 6. Schematic 3D representation of a stack of 11 monomers of **3a**. (*Left*) Side view of the stack; (*Right*) top view.

[†]The dark, ill-defined and larger spots are contamination in the specimen from ice crystal formation.
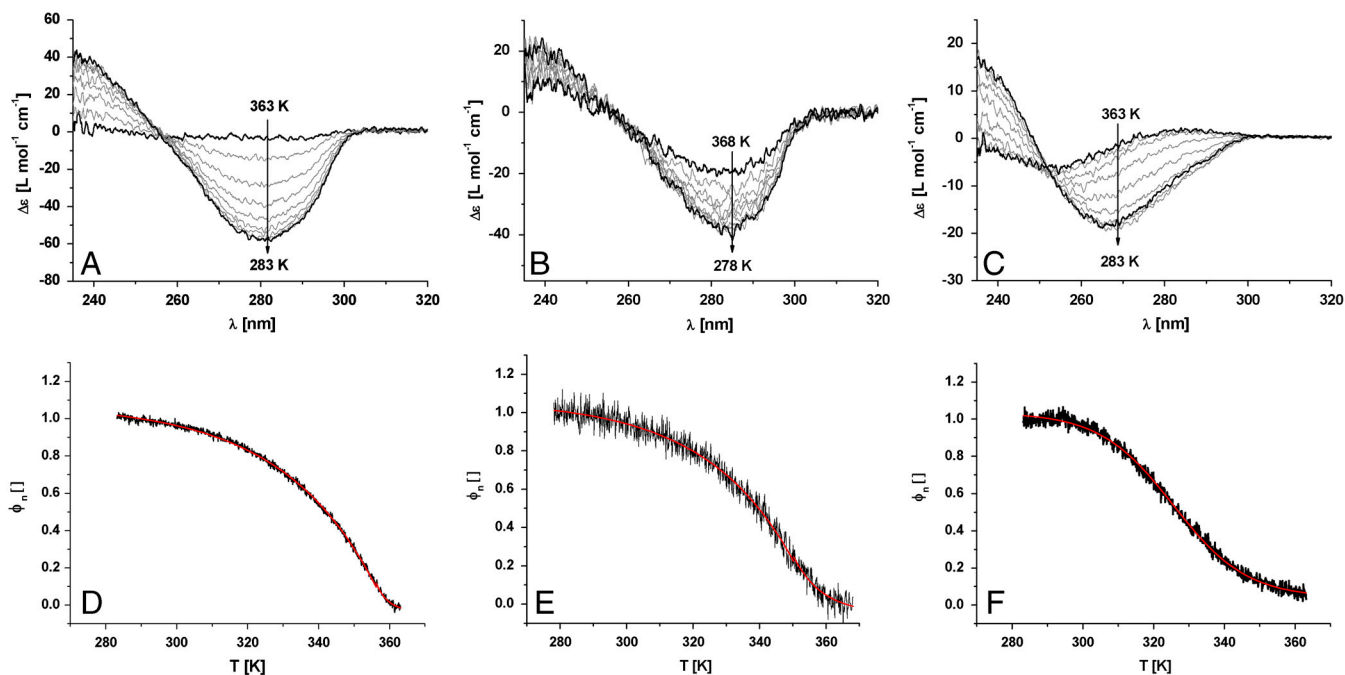
Fig. 7. Temperature-dependent CD spectra in a 100-mM citrate buffer at pH 6: (*A*) discotic **1a** ($5 \cdot 10^{-6}$ M), (*B*) discotic **2a** ($2.5 \cdot 10^{-6}$ M) and discotic **3a** ($20 \cdot 10^{-6}$ M) and the resulting normalized and fitted CD cooling curves monitored at *D* $\lambda = 282$ nm for discotic **1a**, (*E*) $\lambda = 283$ nm for discotic **2a**, (*F*) $\lambda = 269$ nm for discotic **3a**. The lower three graphs show the normalized data as degree of aggregation Φ_n vs. temperature: 0 refers to the molecular dissolved state and 1 to a fully polymerized system; red lines represent the best fits (37, 54).

grand challenges in supramolecular chemistry: controlling the shape and size of functional noncovalent polymers.

In more general terms, cooperativity is an increasingly intriguing concept for chemists (67), and it has become clear that its presence or absence in the self-assembly mechanism is a key feature in manipulating the physical properties of synthetic supramolecular polymers (36). This is in analogy to the central role of cooperativity in many biological systems, such as amyloid fibril proliferation (68, 69), itself linked to clinical disorders ranging from Alzheimer's disease to type II diabetes (70).

Materials and Methods

Unless stated otherwise, all reagents and chemicals were obtained from commercial sources at the highest purity available and used without further purification. Water was demineralized prior to use. Reactions were conducted under an argon atmosphere using standard Schlenk line techniques unless otherwise specified. Flash chromatography was performed on a Biotage flash chromatography system. ^{1}H-NMR, ^{13}C, and ^{19}F-NMR spectra were recorded on Varian Mercury 400 and 200 spectrometers at 298 K. The ^{1}H-DOSY NMR experiments were recorded on a Varian Unity Inova 500 spectrometer equipped with a 5-mm indirect-detection pulsed field gradient (ID-PFG) probe from Varian. Matrix-assisted laser desorption/ionization mass spectra were obtained on a PerSeptive Biosystems Voyager DE-PRO spectrometer. Liquid chromatography-mass spectrometry (LC-MS) analyses were performed using a Shimadzu SCL-10 AD VP series HPLC coupled to a diode array detector

(Finnigan Surveyor PDA Plus detector, Thermo Electron Corporation) and an Ion-Trap (LCQ Fleet, Thermo Scientific). Gd^{III} and Y^{III} contents were determined by means of inductively coupled plasma atomic emission spectrometry (ICP-AES) conducted by the MiPlaza Materials Analysis laboratories (Philips Research Europe) in Eindhoven, The Netherlands. Cryogenic transmission microscopy measurements were performed on the cryoTitan TEM (FEI), equipped with a field emission gun (FEG) operating at 300 kV. Images were recorded using a 2k × 2k Gatan CCD camera equipped with a post column Gatan energy filter (GIF). CD and UV/Vis measurements were performed on a Jasco J-815 spectropolarimeter where the sensitivity, time constant, and scan rate were chosen appropriately. Corresponding temperature-dependent measurements were performed with a Jasco PTC-348WI Peltier-type temperature controller, with a temperature range of 263–383 K and adjustable temperature slope. The SAXS measurements were performed at the Dutch-Belgian BM26B beamline at the European Synchrotron Radiation Facility in Grenoble, France. A sample-to-detector distance of 6.23 m was used together with an X-ray photon wavelength of 1.24 Å. The observed *q* range was 7×10^{-3} Å^{-1} $\leq q \leq 0.12$ Å^{-1}, where *q* is the magnitude of the scattering vector $q = (4\pi/\lambda) \sin\theta$, and where λ is the X-ray wavelength and θ is half of the scattering angle. *SI Appendix* provides all the reaction schemes, detailed experimental procedures and characterization, additional CD and UV/Vis data, as well as ^{1}H-DOSY NMR and SAXS procedures.
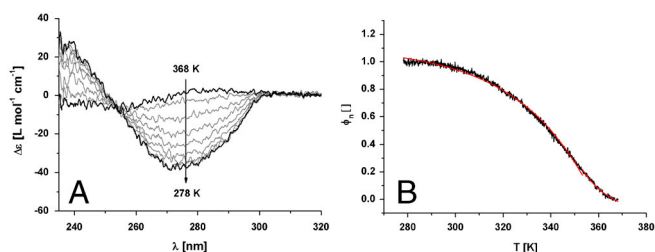

Fig. 8. (*A*) Temperature-dependent CD spectra in a citrate buffer (100 mM, pH 6) and overall NaCl concentration of 0.5 M, of discotic **3a** ($7 \cdot 10^{-6}$ M), and (*B*) the resulting normalized and fitted CD cooling curves monitored at $\lambda = 276$ nm.
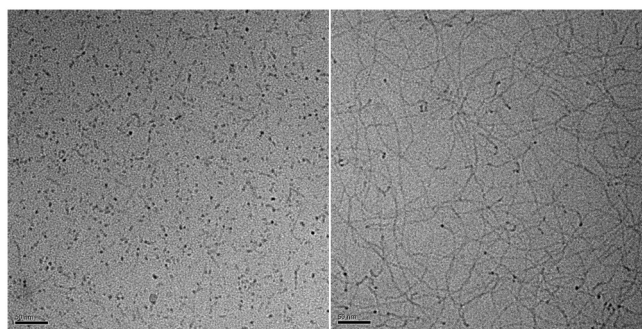

Fig. 9. *Cryo*-TEM micrographs for discotic amphiphile **3a** (1 mM) vitrified at 288 K in citrate buffer (100 mM, pH 6) and overall NaCl concentration of 3 M (*Left*) and 5 M (*Right*); scale bar represents 50 nm.

1. Whitesides GM, Mathias JP (1991) Molecular self-assembly and nanochemistry. *Science* 254:1312–1319.
2. Lehn J-M (1995) *Supramolecular Chemistry* (Wiley-VCH, Weinheim, Germany).
3. Lehn J-M (2002) Toward self-organization and complex matter. *Science* 295:2400–2403.
4. Whitesides GM, Grzybowski B (2002) Self-assembly at all scales. *Science* 295:2418–2421.
5. Förster S, Antonietti M (1998) Amphiphilic block copolymers in structure-controlled nanomaterial hybrids. *Adv Mater* 10:195–217.
6. Rodríguez-Hernández J, Chécot F, Gnanou Y, Lecommandoux S (2005) Toward 'smart' nano-objects by self-assembly of block copolymers in solution. *Prog Polym Sci* 30:691–724.
7. Vriezema DM, et al. (2005) Self-assembled nanoreactors. *Chem Rev* 105:1445–1489.
8. O'Reilly RK, Hawker CJ, Wooley KL (2006) Cross-linked block copolymer micelles: Functional nanostructures of great potential and versatility. *Chem Soc Rev* 35:1068–1083.
9. Blanazs A, Armes SP, Ryan AJ (2009) Self-assembled block copolymer aggregates: from micelles to vesicles and their biological applications. *Macromol Rapid Comm* 30:267–277.
10. Israelachvili JN, Mitchell DJ, Ninha BW (1976) Theory of self-assembly of hydrocarbon amphiphiles into micelles and bilayers. *J Chem Soc Faraday Trans 2* 72:1525–1568.
11. Israelachvili JN, Marčelja S, Horn RG (1980) Physical principles of membrane organization. *Q Rev Biophys* 13:121–200.
12. Zhang L, Eisenberg A (1995) Multiple morphologies of "crew-cut" aggregates of polystyrene-b-poly(acrylic acid) block copolymers. *Science* 268:1728–1731.
13. Bellomo EG, et al. (2004) Stimuli-responsive polypeptide vesicles by conformation-specific assembly. *Nat Mater* 3:244–248.
14. Percec V, et al. (2010) Self-assembly of Janus dendrimers into uniform dendrimersomes and other complex architectures. *Science* 328:1009–1014.
15. Israelachvili J (1991) *Intermolecular & Surface Forces* (Academic, London), 2nd Ed.
16. Gohy J-F (2005) Block copolymer micelles. *Adv Polym Sci* 190:65–136.
17. Denkova AG, Mendes E, Coppens M-O (2010) Non-equilibrium dynamics of block copolymer micelles in solution: Recent insights and open questions. *Soft Matter* 6:2351–2357.
18. Hayward RC, Pochan DJ (2010) Tailored assemblies of block copolymers in solution: It is all about the process. *Macromolecules* 43:3577–3584.
19. Brunsveld L, Folmer BJB, Meijer EW, Sijbesma RP (2001) Supramolecular polymers. *Chem Rev* 101:4071–4097.
20. Hoeben FJM, Jonkheijm P, Meijer EW, Schenning APHJ (2005) About supramolecular assemblies of π-conjugated systems. *Chem Rev* 105:1491–1546.
21. Dankers PYW, Meijer EW (2007) Supramolecular biomaterials. A modular approach towards tissue engineering. *Bull Chem Soc Jpn* 80:2047–2073.
22. Palmer LC, Velichko YS, Olvera de la Cruz M, Stupp SI (2007) Supramolecular self-assembly codes for functional structures. *Philos Trans R Soc London A* 365:1417–1433.
23. Yamamoto Y, et al. (2006) Photoconductive coaxial nanotubes of molecularly connected electron donor and acceptor layers. *Science* 314:1761–1764.
24. Feng X, et al. (2009) Towards high charge-carrier mobilities by rational design of the shape and periphery of discotics. *Nat Mater* 8:421–426.
25. Yin M, et al. (2009) Functionalization of self-assembled hexa-peri-hexabenzocoronene fibers with peptides for bioprobing. *J Am Chem Soc* 131:14618–14619.
26. Müller MK, Brunsveld L (2009) A supramolecular polymer as a self-assembling polyvalent scaffold. *Angew Chem Int Edit* 48:1–5.
27. Stupp SI, et al. (1997) Supramolecular materials: Self-organized nanostructures. *Science* 276:384–389.
28. Dong H, et al. (2007) Self-assembly of multidomain peptides: Balancing molecular frustration controls conformation and nanostructure. *J Am Chem Soc* 129:12468–12472.
29. Palmer LC, Stupp SI (2008) Molecular self-assembly into one-dimensional nanostructures. *Acc Chem Res* 41:1674–1684.
30. Janssen PGA, et al. (2007) ssDNA templated self-assembly of chromophores. *J Am Chem Soc* 129:6078–6079.
31. Bull SR, et al. (2008) A templating approach for monodisperse self-assembled organic nanostructures. *J Am Chem Soc* 130:2742–2743.
32. Lortie F, et al. (2005) Chain stopper-assisted characterization of supramolecular polymers. *Macromolecules* 38:5283–5287.
33. Wang X, et al. (2007) Cylindrical block copolymer micelles and co-micelles of controlled length and architecture. *Science* 317:644–647.
34. Bishop KJM, Wilmer CE, Soh S, Grzybowski BA (2009) Nanoscale forces and their uses in self-assembly. *Small* 5:1600–1630.
35. Cui H, et al. (2010) Spontaneous- and X-ray-triggered Crystallization at long range in self-assembling filament networks. *Science* 327:555–559.
36. De Greef TFA, et al. (2009) Supramolecular polymerization. *Chem Rev* 109:5687–5754.
37. Smulders MMJ, et al. (2010) How to distinguish isodesmic from cooperative supramolecular polymerisation. *Chem Eur J* 16:362–367.
38. Mukerjee P, Mysels KJ, Kapauan P (1967) Counterion specificity in the formation of ionic micelles-size, hydration, and hydrophobic bonding effects. *J Phys Chem* 71:4166–4175.
39. Tanford C (1974) Theory of micelle formation in aqueous solutions. *J Phys Chem* 78:2469–2479.
40. van den Hout KP, Martin-Rapún R, Vekemans JA, Meijer EW (2007) Tuning the stacking properties of C_3-symmetrical molecules by modifying a dipeptide motif. *Chem-Eur J* 13:8111–8123.
41. Smulders MMJ, Schenning APHJ, Meijer EW (2008) Insight into the mechanisms of cooperative self-assembly; the "sergeants-and-soldiers" principle of chiral and achiral C_3-symmetrical discotic triamides. *J Am Chem Soc* 130:606–611.
42. Stals PJM, et al. (2009) Asymmetrically substituted benzene-1,3,5-tricarboxamides: Self-assembly and odd-even effects in the solid state and in dilute solution. *Chem-Eur J* 15:2071–2080.
43. Guinier A, Fournet G (1955) *Small-Angle Scattering of X-Rays* (Chapman & Hall, London).
44. Glatter O, Kratky O (1982) *Small Angle X-Ray Scattering* (Academic, London).
45. Arnaud A, et al. (2004) Aqueous supramolecular polymer formed from an amphiphilic perylene derivative. *Angew Chem Int Edit* 43:1718–1721.
46. Ozbas B, Rajagopal K, Schneider JP, Pochan DJ (2004) Semiflexible chain networks formed via self-assembly of β-hairpin molecules. *Phys Rev Lett* 93:268106.
47. Li Z, et al. (2010) Structure and gelation mechanism of tunable guanosine-based supramolecular hydrogels. *Langmuir* 26:10093–10101.
48. Li D, Kagan G, Hopson R, Williard PG (2009) Formula weight prediction by internal reference diffusion-ordered NMR spectroscopy (DOSY). *J Am Chem Soc* 131:5627–5634.
49. Corbin PS, et al. (2002) Discrete and polymeric self-assembled dendrimers: Hydrogen bond-mediated assembly with high stability and high fidelity. *Proc Natl Acad Sci USA* 99:5099–5104.
50. Percec V, et al. (2006) Synthesis and retrostructural analysis of libraries of AB3 and constitutional isomeric AB2 phenylpropyl ether-based supramolecular dendrimers. *J Am Chem Soc* 128:3324–3334.
51. Jonkheijm P, van der Schoot P, Schenning APHJ, Meijer EW (2006) Probing the solvent-assisted nucleation pathway in chemical self-assembly. *Science* 313:80–83.
52. Chen Z, Lohr A, Saha-Möller CR, Würthner F (2009) Self-assembled π-stacks of functional dyes in solution: Structural and thermodynamic features. *Chem Soc Rev* 38:564–584.
53. Palmans ARA, Meijer EW (2007) Amplification of chirality in dynamic supramolecular assemblies. *Angew Chem Int Edit* 47:8948–8968.
54. van der Schoot P (2005) *Supramolecular Polymers*, ed A Ciferri (Taylor & Francis, London), pp 77–106.
55. Martin RB (1996) Comparisons of indefinite self-association models. *Chem Rev* 96:3043–3064.
56. Zhao D, Moore JS (2003) Nucleation–elongation: A mechanism for cooperative supramolecular polymerization. *Org Biomol Chem* 1:3471–3491.
57. Imae T, Ikeda S (1987) Characteristics of rod-like micelles of cetyltrimethylammonium chloride in aqueous NaCl solutions: Their flexibility and the scaling laws in dilute and semidilute regimes. *Colloid Polym Sci* 265:1090–1098.
58. MacKintosh FC, Safran SA, Pincus PA (1990) Self-assembly on linear aggregates: The effect of electrostatics on growth. *Europhys Lett* 12:697–702.
59. Safran SA, Pincus PA, Cates ME, MacKintosh FC (1990) Growth of charged micelles. *J Phys (Paris)* 51:503–510.
60. Manning GS (1969) Limiting laws and counterion condensation in polyelectrolyte solutions I. Colligative properties. *J Chem Phys* 51:924–933.
61. de Gennes P-G, Pincus P, Velasco RM, Brochard F (1976) Remarks on polyelectrolyte conformation. *J Phys (Paris)* 37:1461–1473.
62. Odijk T (1977) Polyelectrolytes near the rod limit. *J Polym Sci Pol Phys* 15:477–483.
63. Skolnick J, Fixman M (1977) Electrostatic persistence length of a wormlike polyelectrolyte. *Macromolecules* 10:944–948.
64. Khokhlov AR (1980) Collapse of weakly charged poly-electrolytes. *J Phys A* 13:979–987.
65. Dobrynina AV, Rubinstein M (2005) Theory of polyelectrolytes in solutions and at surfaces. *Prog Polym Sci* 30:1049–1118.
66. Kegel WK, van der Schoot P (2004) Competing hydrophobic and screened-Coulomb interactions in hepatitis B virus capsid assembly. *Biophys J* 86:3905–3913.
67. Hunter CA, Anderson HL (2009) What is cooperativity? *Angew Chem Int Edit* 48:7488–7499.
68. Ruschak AM, Miranker AD (2007) Fiber-dependent amyloid formation as catalysis of an existing reaction pathway. *Proc Natl Acad Sci USA* 104:12341–12346.
69. Knowles TPJ, et al. (2009) An analytical solution to the kinetics of breakable filament assembly. *Science* 326:1533–1537.
70. Chiti F, Dobson CM (2006) Protein misfolding, functional amyloid, and human disease. *Annu Rev Biochem* 75:333–366.

CHEMISTRY